Activation of Smad2/3 signaling by low fluid shear stress mediates artery inward remodeling

Hanqiang Deng[a,1], Elizabeth Min[a,b,1], Nicolas Baeyens[a,c,d,2], Brian G. Coon[a], Rui Hu[a], Zhen W. Zhuang[a,e], Minghao Chen[a], Billy Huang[a], Titilayo Afolabi[a], Georgia Zarkada[a], Angela Acheampong[d], Kathleen McEntee[d], Anne Eichmann[a,c,e], Fang Liu[f,g,h,i], Bing Su[j,k,l], Michael Simons[a,b,c], and Martin A. Schwartz[a,b,c,m,2]

[a]Yale Cardiovascular Research Center, Yale School of Medicine, New Haven, CT 06511; [b]Department of Cell Biology, Yale School of Medicine, New Haven, CT 06511; [c]Department of Internal Medicine (Cardiology), Yale School of Medicine, New Haven, CT 06511; [d]Laboratoire de Physiologie et Pharmacologie, Faculty of Medicine, Université libre de Bruxelles, 1050 Bruxelles, Belgium; [e]Department of Physiology, Yale School of Medicine, New Haven, CT 06511; [f]Center for Advanced Biotechnology and Medicine, Rutgers, The State University of New Jersey, New Brunswick, NJ 08901-8554; [g]Susan Lehman Cullman Laboratory for Cancer Research, Rutgers, The State University of New Jersey, New Brunswick, NJ 08901-8554; [h]Ernest Mario School of Pharmacy, Rutgers, The State University of New Jersey, New Brunswick, NJ 08901-8554; [i]Rutgers Cancer Institute of New Jersey, Rutgers, The State University of New Jersey, New Brunswick, NJ 08901-8554; [j]Shanghai Institute of Immunology, Shanghai Jiao Tong University School of Medicine, Shanghai 200240, China; [k]Department of Microbiology and Immunology, Shanghai Jiao Tong University School of Medicine, Shanghai 200240, China; [l]Ministry of Education Key Laboratory of Cell Death and Differentiation, Shanghai Jiao Tong University School of Medicine, Shanghai 200240, China; and [m]Department of Biomedical Engineering, Yale University, New Haven, CT 06520

Endothelial cell (EC) sensing of wall fluid shear stress (FSS) from blood flow governs vessel remodeling to maintain FSS at a specific magnitude or set point in healthy vessels. Low FSS triggers inward remodeling to restore normal FSS but the regulatory mechanisms are unknown. In this paper, we describe the signaling network that governs inward artery remodeling. FSS induces Smad2/3 phosphorylation through the type I transforming growth factor (TGF)-β family receptor Alk5 and the transmembrane protein Neuropilin-1, which together increase sensitivity to circulating bone morphogenetic protein (BMP)-9. Smad2/3 nuclear translocation and target gene expression but not phosphorylation are maximal at low FSS and suppressed at physiological high shear. Reducing flow by carotid ligation in rodents increases Smad2/3 nuclear localization, while the resultant inward remodeling is blocked by the EC-specific deletion of Alk5. The flow-activated MEKK3/Klf2 pathway mediates the suppression of Smad2/3 nuclear translocation at high FSS, mainly through the cyclin-dependent kinase (CDK)-2-dependent phosphosphorylation of the Smad linker region. Thus, low FSS activates Smad2/3, while higher FSS blocks nuclear translocation to induce inward artery remodeling, specifically at low FSS. These results are likely relevant to inward remodeling in atherosclerotic vessels, in which Smad2/3 is activated through TGF-β signaling.

hemodynamics | vascular remodeling | MEKK | KLF2 | cyclin-dependent kinase-2

The vertebrate vascular system is designed to match local perfusion to metabolic demands in each tissue, thus optimizing function and ultimately survival. For example, hypoxia induces secretion of factors that dilate small resistance vessels on short time scales and, on longer time scales, factors that stimulate angiogenesis (1). These adjustments increase flow through the larger arteries that feed the affected tissue, inducing their outward remodeling. Conversely, disuse or atrophy of a tissue results in decreased vessel density and inward remodeling of the feeder arteries (2).

Endothelial cells (ECs) that line the inner surfaces of blood vessels transduce signals from hemodynamic wall fluid shear stress (FSS) to regulate vessel remodeling (3). Multiple studies have shown that surgical interventions to increase or decrease flow through an artery stimulate outward or inward remodeling, respectively (4, 5). Current evidence supports a model in which the endothelium encodes an FSS set point that mediates homeostasis (6). Sustained FSS above or below this value induces outward or inward remodeling, thereby restoring FSS to its original value. By contrast, FSS near the setpoint stabilizes vessels. The set point varies for different types of ECs, corresponding to the physiological level of shear stress appropriate to the specific vessel type. For human umbilical vein ECs (HUVECs), physiological FSS in the range of 10 to 20 dynes/cm^2 suppressed inflammatory NF-κB, whereas Smad1/5 is maximally activated in this range. This last result suggests a role for the TGF-β/BMP family ligands and receptors in the shear stress regulation of vascular homeostasis (6).

Signaling by transforming growth factor (TGF)-β/bone morphogenetic protein (BMP) family members regulates cellular responses, including proliferation, differentiation, and migration from early developmental stages to adult life and disease (7). Homologous ligands initiate the activation from three subfamilies: TGF-βs, BMPs, and activins (8). These proteins bind to type I and type II transmembrane receptors that contain cytoplasmic serine/threonine kinase domains. Nonkinase type III receptors sometimes facilitate ligand binding and signaling. Ligand binding initiates receptor activation and C-terminal phosphorylation of receptor-regulated Smads (R-Smads). R-Smad C-terminal phosphorylation promotes their binding to the common Smad, Smad4, and nuclear entry of this complex, which directly binds target gene promoters to regulate gene expression. As Smads are continuously shuttled in and out of

Significance

This paper analyzes the signaling network that regulates the size of artery lumens and thus their ability to transport blood to tissues. Lumen diameter is under close homeostatic regulation to match artery flow to the needs of downstream tissues. However, in atherosclerosis, this regulation is compromised, resulting in restricted blood flow and tissue ischemia. The elucidation of a Smad2/3 pathway that is specifically activated at low flow to trigger inward remodeling and thus restore normal shear stress levels not only reveals a mechanism of physiological regulation but also explains how activation of the same pathway by inflammatory factors in diseased arteries can lead to artery restriction.

the nucleus, nuclear accumulation correlates with their activation (i.e., induction of target genes) (9, 10).

Our previous work showed that the activation and nuclear translocation of Smad1/5 near the physiological set point was triggered by its receptors Alk1 and endoglin (11). Activation by flow was mediated by an ~20-fold increase in sensitivity to the circulating TGF-β family ligands BMP9 and BMP10. Consistent with a role in vascular stabilization, mutation or deletion of these receptors induces vascular malformations that are fragile and prone to rupture (12). Additional studies showed that the related Smad2/3 pathway is also activated by flow, but, in this case, activation was suppressed by physiological laminar FSS and activated by oscillatory FSS, typical of atherosclerosis-susceptible regions of arteries (13, 14). These results prompted us to examine the role of Smad2/3 signaling in flow-dependent vascular remodeling.

Results

Smad2/3 Activation by Shear Stress. Treatment of HUVECs with FSS ranging from 1 to 30 dynes/cm^2 for 12 h induced Smad2/3 nuclear translocation that was maximal under low FSS (1 to 5 dynes/cm^2) and then decreased significantly as FSS reached the physiological range (≥12 dynes/cm^2; Fig. 1 A and B). Parallel assessment of cell alignment (Fig. 1C) confirmed the expected dose response to FSS. qPCR of two direct Smad2/3 target genes, fibronectin and integrin α5 [determined as direct Smad2/3 target genes in a chromatin immunoprecipitation assay with antibody to Smad2 (15)], showed that their expression followed a similar dose dependence, with a maximum at low FSS (Fig. 1 D and E). This response was blocked by small interfering RNA (siRNA)–mediated depletion of Smad2/3 (depletion in *SI Appendix*, Fig. S1), confirming their dependence on Smad2/3 activity. Thus, Smad2/3 signaling in ECs shows biphasic regulation with a maximum at low FSS.

Smad2/3 Phosphorylation. TGF-β receptors typically initiate R-Smad signaling through C-terminal phosphorylation of critical serine residues (9, 10). We, therefore, examined the effects of shear stress intensity (1 to 30 dynes/cm^2) on Smad2/3 C-terminal phosphorylation (p-Smad2/3 C) over a time course of 12 h. p-Smad2/3 peaked around 2 to 4 h after the onset of flow and then decreased to a plateau that was above baseline (Fig. 1F). However, unlike nuclear translocation, p-Smad2/3 showed no evidence of a decrease at high FSS. Thus, while flow induces p-Smad2/3 C, it does not show the same biphasic dependence on FSS magnitude as nuclear translocation. The suppression of nuclear localization and gene induction at high FSS must therefore involve a distinct mechanism.

Identification of Receptors. Our previous work identified Alk1 and endoglin as key mediators of flow-induced Smad1/5/8 activation (11). To determine which receptors mediate flow activation of Smad2/3, we first considered Alk5 (TGFβR1), the major type I receptor for TGF-β. For comparison, we examined Alk1 and endoglin as well. The depletion of Alk5 in HUVECs inhibited flow-stimulated p-Smad2/3 C, which was rescued by reexpression of siRNA-resistant Alk5 (Fig. 2 A and B). The depletion of Alk1 or endoglin had no detectable effect on Smad2/3 activation. We also considered Neuropilin-1 (Nrp1), based on a recent report that it interacts with Alk1 and Alk5 (16), and its involvement with the FSS activation of VEGFR2 (17, 18). Depleting Nrp1 reduced p-Smad2/3 C by flow, which was rescued by its reexpression (Fig. 2 A and C). Nrp1 depletion, however, had no effect on p-Smad2/3 C induced by its soluble ligand, BMP9, in the absence of flow (*SI Appendix*, Fig. S2A). The depletion of Alk5 or Nrp1 also blocked Smad2/3 nuclear translocation (*SI Appendix*, Fig. S2B). Alk5 and Nrp1 are thus the key receptors required for the flow activation of Smad2/3, as Alk1 and endoglin are for the flow activation of Smad1/5 (11).

Identification of Ligands. By analogy to the requirement for BMP9 or BMP10 in the flow activation of Smad1/5 (11), we next addressed

the role of soluble ligands. FSS failed to activate Smad2/3 in cells in serum-free medium (control lanes in Fig. 2D and *SI Appendix*, Fig. S3A), indicating that a circulating factor (or factors) is required. TGF-β is the primary Alk5 ligand that stimulates Smad2/3 activation. However, TGF-β2 at concentrations from 1 pg/mL to 10 ng/mL showed no synergy with shear stress. Indeed, there was a trend toward slightly lower Smad2/3 activation under flow (*SI Appendix*, Fig. S3A). As Smad1/5 activation by BMP9 or BMP10 was enhanced by flow, we next tested these ligands. Flow induced a leftward shift in the dose–response curve for BMP9-induced Smad2/3 activation by about 10-fold, similar to the effect on Smad1/5 activation (Fig. 2D). BMP9 was also required for Smad2/3 nuclear translocation in response to flow (*SI Appendix*, Fig. S3B), as expected. To our surprise, flow did not affect the response to BMP10 (*SI Appendix*, Fig. S3C). To confirm these findings, we added BMP-blocking antibodies to medium containing 2% serum as the source of soluble ligands. Anti-BMP9 IgG reduced flow-induced phosphorylation of both Smad1/5 and Smad2/3 (Fig. 2 E, *Left*). By contrast, anti-BMP10 only reduced flow-induced p-Smad1/5 (Fig. 2 E, *Right*). FSS enhancement of Smad2/3 activation is thus due to increased sensitivity to BMP9 but not related ligands.

Low, Flow-Induced Inward Remodeling In Vivo. We next examined low flow-mediated inward remodeling in vivo using a partial carotid ligation model (19). This model leaves open the occipital artery (OA) rather than the superior thyroid artery (STA); thus, it is distinct from protocols for generating oscillatory flow (20). The ligation of two of the branches of the carotid (Fig. 3A) sharply reduced flow (*SI Appendix*, Fig. S4), which typically results in intimal–medial thickening and a 30 to 40% decrease in the lumen area (Fig. 3B). There is also a compensatory increase in the contralateral carotid flow, but outward remodeling is much less (19). We first addressed whether low FSS activated Smad2/3 in vivo. Carotid ligation in both mice (Fig. 3 C and D) and rats (*SI Appendix*, Fig. S5) increased Smad2/3 nuclear staining in ECs upstream from the closure. This effect in mice was diminished by EC-specific knockout (ECKO) of Alk5, achieved via tamoxifen injection of Cdh5:Cre-ERT2, Alk5$^{fl/fl}$ mice. Thus, Smad2/3 is activated by low FSS in vivo, which required Alk5.

We next asked whether blocking Smad2/3 activation reduces low, flow-induced artery inward remodeling. At day 14 after surgery, arteries were harvested, stained with hematoxylin and eosin, and lumen circumference measured. Whereas wild-type mice the right carotid artery circumference decreased by 18% (P < 0.0039), corresponding to a 33% decrease in area, there was no significant change in Alk5 ECKO mice (Fig. 3E). Altogether, these data demonstrate that Alk5-Smad2/3 signaling is required for low, flow-induced inward artery remodeling.

Suppression at High FSS. The biphasic activation of Smad2/3 by flow suggests that another pathway activated at higher FSS antagonizes p-Smad2/3 nuclear translocation. The accompanying manuscript (21) reports that the ECKO of MEKK3 in mice triggers spontaneous inward arterial remodeling through the activation of the TGFβR1–Smad2/3 pathway. MEKK2 and MEKK3 are upstream components in the pathway that induces expression of the transcription factor Klf2 at high FSS (22). This pathway mediates the expression of eNOS and other genes that promote vasodilation and stabilize the vasculature. We therefore examined the effects of siRNA-mediated depletion of MEKK3 (confirmed in *SI Appendix*, Fig. S6A) on the flow activation of Smad2/3 signaling. MEKK3 knockdown (KD) had little effect at low shear but eliminated the suppression of Smad2/3 nuclear translocation at high FSS (Fig. 4 A and B). Similar effects were observed in mouse aortic ECs (*SI Appendix*, Fig. S7). Thus, MEKK3 is required for the high-flow suppression of Smad2/3 function.

We next tested the role of Klf2 in this pathway. Following KD of Klf2 (confirmed in *SI Appendix*, Fig. S6B), ECs were subjected to
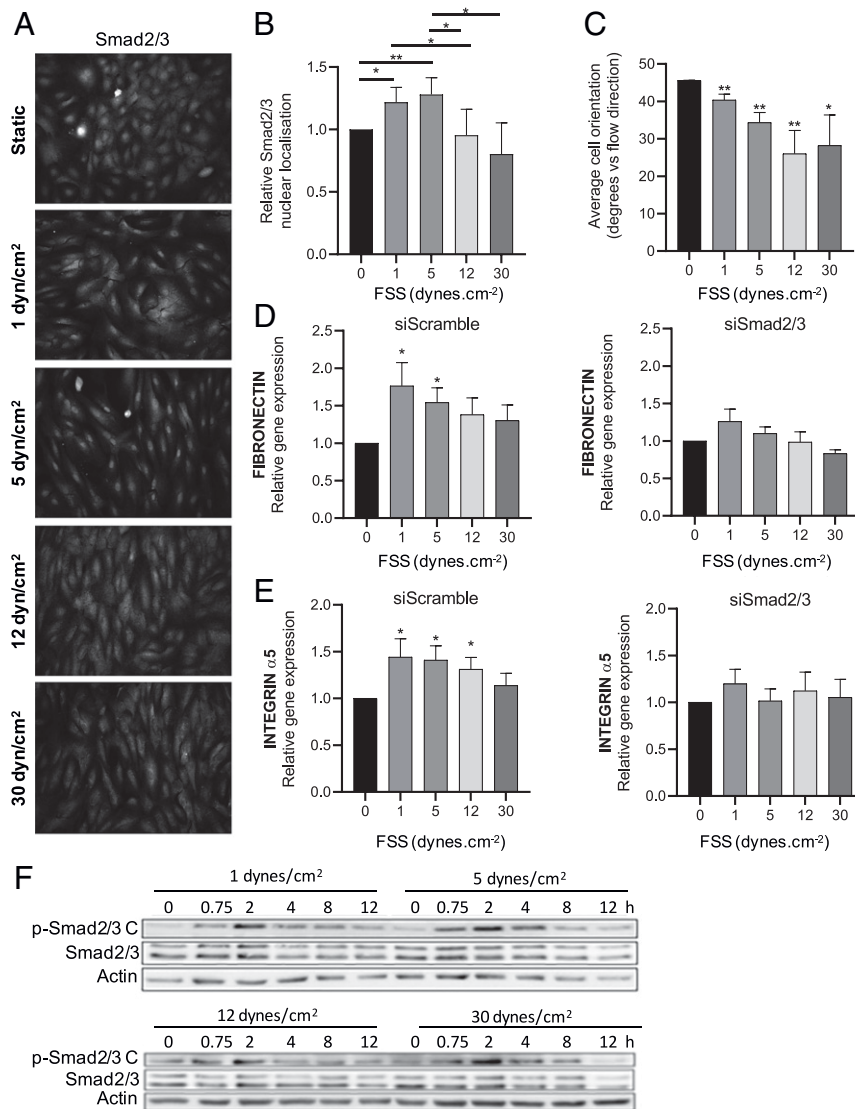
Fig. 1. Smad2/3 regulation by shear stress. (*A*) HUVECs were exposed to laminar FSS at the indicated magnitudes for 12 h, fixed, and stained for Smad2/3. (*B*) Quantification of Smad2/3 nuclear localization, $n = 4$. (*C*) Cell alignment was quantified by measuring the angle between the direction of flow and the long axis of the cell; $n = 4$. (*D* and *E*) Fibronectin and integrin α5 mRNA levels were assessed by qPCR; $n = 4$. (*F*) HUVECs were exposed to laminar FSS at the indicated magnitudes for 12 h. p-Smad2/3 C was assessed by the Western blotting of cell lysates. Similar results were obtained in three independent experiments. Quantified values are means ± SEM, *$P < 0.05$, and **$P < 0.01$, calculated by one-way ANOVA with Tukey's multiple comparison tests.

FSS at different magnitudes. Klf2 depletion similarly had little effect at low FSS but prevented the suppression of Smad2/3 at high FSS (Fig. 4 *C* and *D*). The best studied gene target of the MEKK3-Klf2 axis is eNOS (NOS3), which is a critical mediator of vasodilation and therefore a top candidate for opposing inward remodeling. eNOS is a well-validated Klf2 target gene that has been implicated in the regulation of artery lumen diameter (23, 24). Two different siRNAs against eNOS gave nearly complete KD of eNOS but had no effect on Smad2/3 nuclear localization in high flow (*SI Appendix*, Fig. S8). This result implies that other target genes must mediate the repressive effect on Smad2/3 activity. However, Klf2 regulates the expression of hundreds of EC genes (25), making identification challenging. We therefore decided to look more closely into the mechanism of nuclear exclusion at high shear.

Smad2/3 Linker Phosphorylation. An important mechanism of Smad2/3 inhibition involves the phosphorylation of serine and threonine residues in the "linker" region that connects the N-terminal MH1 and C-terminal MH2 domains (26). We therefore measured

Smad2/3 linker phosphorylation at low and high FSS by Western blotting with specific antibodies (27). These experiments revealed large increases in phosphorylation at multiple linker region serines under high FSS (Fig. 5 *A* and *B*). To determine whether this mechanism mediates nuclear exclusion at high shear, we transfected cells with Smad3 bearing mutations in the four critical residues. This mutant ("EPSM") remained nuclear at high shear (Fig. 5 *C* and *D*). Next, we tested the role of MEKK3 and Klf2 in linker phosphorylation. The depletion of either protein reduced high shear-induced linker phosphorylation (Fig. 6 *A–D*). Together, these data show that Smad2/3 linker phosphorylation induced by high flow through the MEKK3-Klf2 pathway mediates the inhibition of Smad2/3 nuclear translocation at high shear.

CDK2 Is Required for Linker Phosphorylation. Known Smad linker region kinases include mitogen-activated protein kinases (Erk, Jnk, and p38); cyclin-dependent kinases (CDKs); Rho-associated protein kinase, Akt; calcium calmodulin-dependent kinase; and glycogen synthase kinase-3 (26, 28). To narrow down the search,
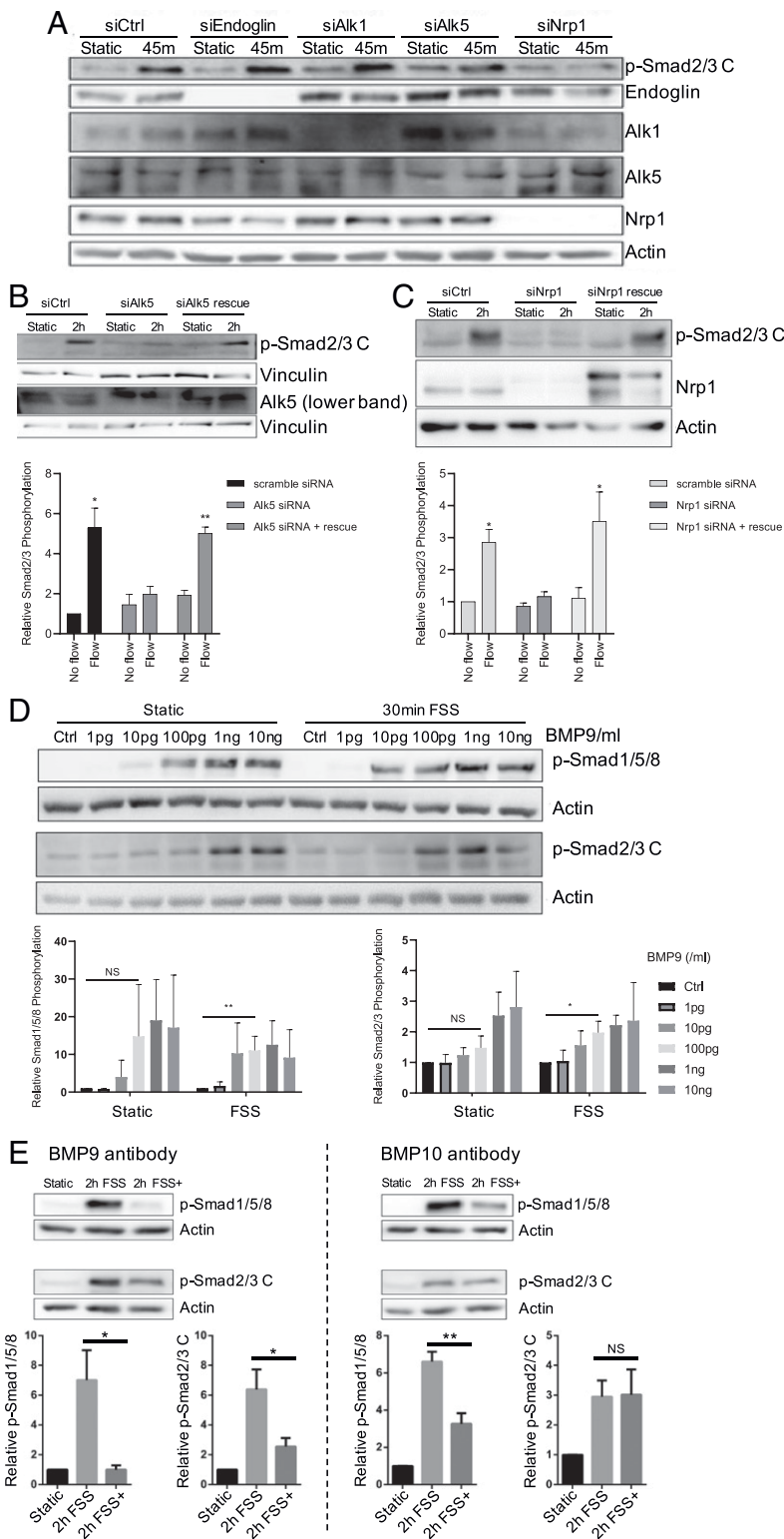
Deng et al.
Activation of Smad2/3 signaling by low fluid shear stress mediates artery inward remodeling

PNAS | 3 of 12
https://doi.org/10.1073/pnas.2105339118

Fig. 2. Identification of receptors and ligands required for flow-induced Smad2/3 activation. (*A*) ECs were subject to KD of the indicated receptors and exposed to flow (12 dynes/cm²); activation of Smad2/3 was assayed by Western blotting. (*B*) Alk5 KDs were rescued by reexpression of siRNA-resistant Alk5 and flow activation of Smad2/3 assayed; $n = 3$. (*C*) Nrp1 KD was rescued by reexpression of siRNA-resistant Nrp1 and flow activation of Smad2/3 assayed. For quantification, $n = 3$. (*D*) ECs were stimulated by the addition of BMP9 in the presence or absence of FSS at 12 dynes/cm² for 30 min, and p-Smad2/3 was assayed by Western blotting; $n = 3$. (*E*) HUVECs in 2% serum were exposed to laminar FSS for 2 h without (2 h FSS) or with (2 h FSS+) blocking antibodies to BMP9 ($n = 4$) or BMP10 ($n = 3$), as indicated. Samples were then assayed for p-Smad. Quantified values are means ± SEM *$P < 0.05$, **$P < 0.01$, and NS: not significant, calculated by one-way ANOVA with Tukey's multiple comparison tests.
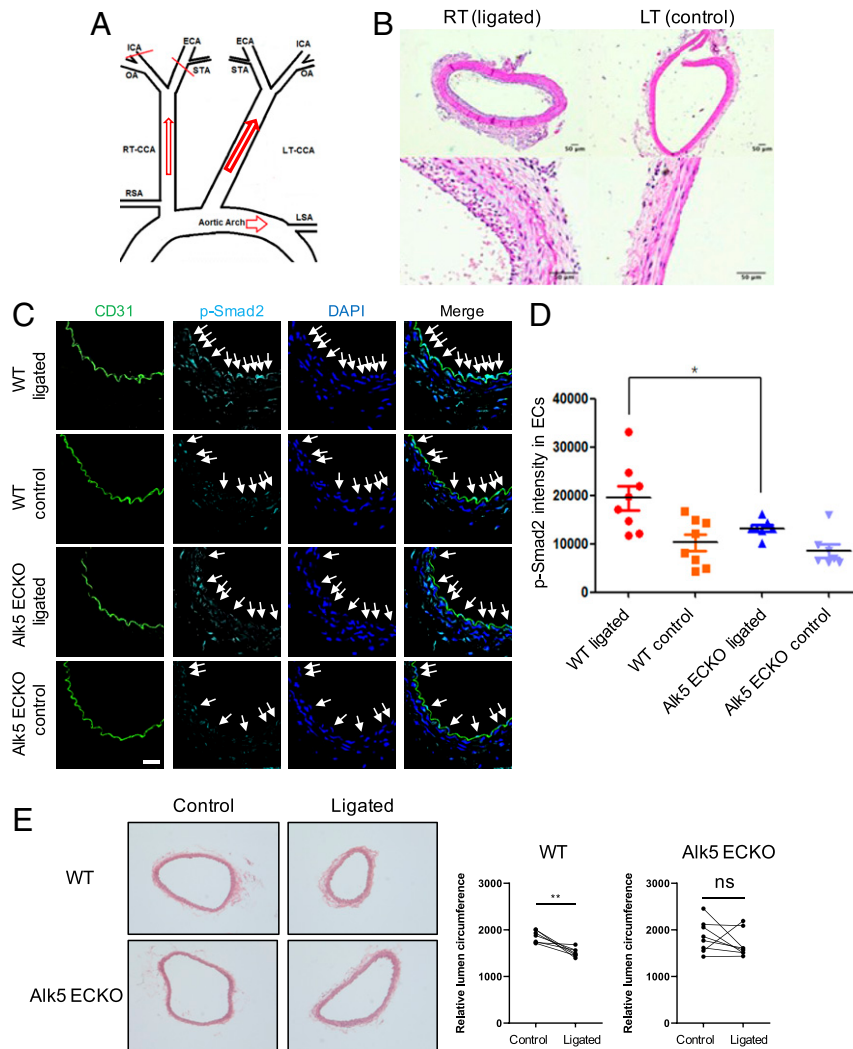
Fig. 3. Low flow-induced inward remodeling in vivo. (*A*) Schematic of carotid ligation: Three branches of the right common carotid artery (RCA), the external carotid artery (ECA), internal carotid artery (ICA), and the STA were ligated, leaving the OA open. RT, right, LT, left. (*B*) Carotid ligation, as illustrated in Fig. 5*A*, was performed on the right side of wild-type (WT) or ALK5 ECKO mice, with the left side used as a control. Transverse sections of paraffin-embedded common carotid arteries were stained with hematoxylin and eosin. (*C*) Immunostaining for p-Smad2 and CD31 in ligated right or control left carotid arteries from WT and Alk5 ECKO mice. Arrowheads are the nuclei- and p-Smad2–positive areas in artery ECs. (Scale bar, 50 μm.) (*D*) Quantification of p-Smad2 intensity in ECs. $n = 8$ and $*P < 0.05$, calculated by one-way ANOVA with Tukey's multiple comparison tests. (*E*) Mice with or without the EC-specific deletion of Alk5 were subject to right carotid ligation and vessel circumference for both ligated right side and control left side assessed at 2 wk. $**P < 0.01$ and ns: not significant, calculated by unpaired t tests.

we performed RNA sequencing (RNAseq) on HUVECs after Klf2 KD. None of these kinases changed significantly. We noticed, however, that two CDK inhibitors, CDKN2B and CDKN1A, markedly increased after Klf2 KD (Fig. 7*A*); this result implies that they are suppressed by Klf2 and predicts that the targeted CDKs would be activated in high shear and thus might mediate the observed Smad linker phosphorylation. Several cyclins also decreased in the Klf2 KD, consistent with lower-CDK activity. As an initial test of this hypothesis, we used two chemical inhibitors that target a number of CDKs, AT7519 (29) and flavopiridol (30). Concentrations of these compounds that preferentially target CDKs potently reversed the inhibition of Smad2/3 nuclear localization at high shear with minimal effects in no or in low flow (*SI Appendix*, Fig. S9 *A* and *B*). The CDK inhibitors also blocked Smad2/3 linker phosphorylation (*SI Appendix*, Fig. S9 *C* and *D*). Recent work suggests that arterial ECs under high FSS are in late G1 arrest (31), suggesting activation of CDK4 or CDK2. Flavopiripol targets these isoforms, though it also inhibits CDK9 (32). To test the possible involvement of CDK9, cells were treated with AZD4573, which

targets mainly CDK9 (33). This inhibitor had no effect on Smad2/3 linker phosphorylation (*SI Appendix*, Fig. S9E). We, therefore, focused on CDK2 and CDK4.

To identify the specific CDK responsible, CDK2 and CDK4 were depleted in HUVECs using siRNA (Fig. 7*B*). KD of CDK2 strongly blocked nuclear exclusion in cells under high shear, whereas CDK4 KD had little effect (Fig. 7 *C* and *D*). Additionally, CDK2 KD blocked linker phosphorylation (Fig. 7 *E* and *F*). To complement these findings, we assayed CDK2 activity using a reporter construct whose phosphorylation by CDK2 results in translocation out of the nucleus (34). This assay showed that high FSS induced nuclear exclusion of the reporter (i.e., activated CDK2), which was blocked by Klf2 depletion (Fig. 7*G*). A time course, however, showed that CDK2 activation was negligible at 45 min, requiring about 2 h to manifest (*SI Appendix*, Fig. S10). Taking these and previous results together, we conclude that the Klf2-dependent activation of CDK2 is the major cause of Smad2/3 linker phosphorylation and nuclear exit after a few hours of flow.
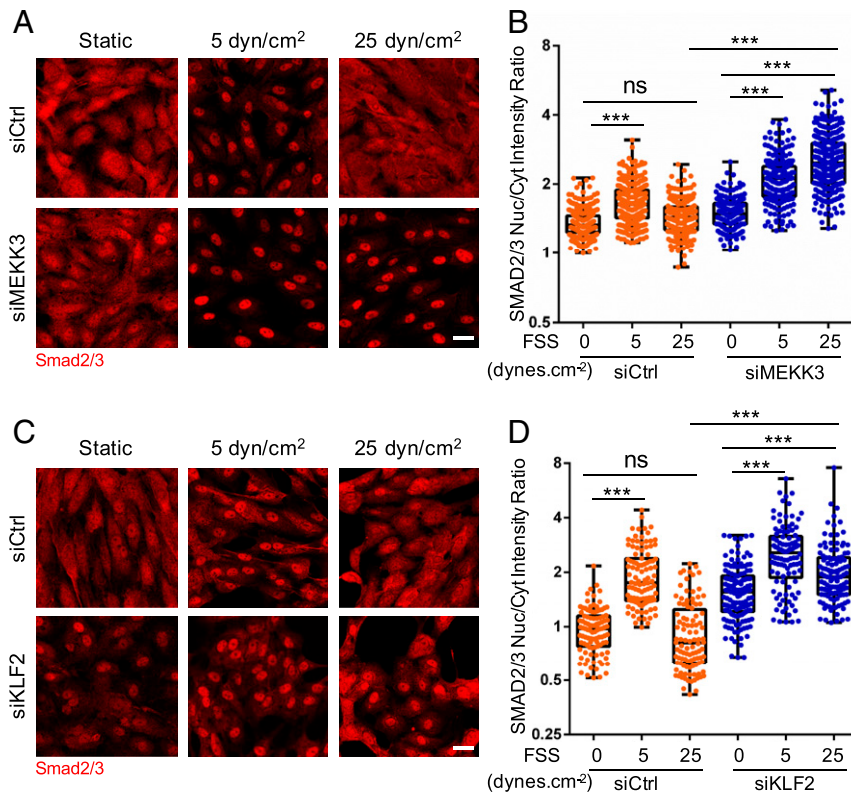
Deng et al.
Activation of Smad2/3 signaling by low fluid shear stress mediates artery inward remodeling

PNAS | 5 of 12
https://doi.org/10.1073/pnas.2105339118

Fig. 4. MEKK3 and Klf2 suppress Smad2/3 at high FSS. (*A*) HUVECs transfected with control (Ctrl) or MEKK3 siRNA were subjected to FSS at the indicated magnitude for 12 h. Cells were fixed and stained for Smad2/3. Panels show representative images, which are quantified in *B*. Values are means ± SEM. (*C*) HUVECs were transfected with Ctrl or KLF2 siRNA, subjected to FSS, then fixed and stained for Smad2/3, as in *A*. (*D*) Results from *C* were quantified as in *B*. (Scale bar, 50 μm.) *n* = 100 to 150 cells for each group from three independent experiments. ***P < 0.001 and ns: not significant, calculated by one-way ANOVA with Tukey's multiple comparison tests.

However, results also suggest that MEKK3 mediates the effect at early times independent of Klf2 and Cdk2 (*Discussion*).

We next assessed the roles of the Klf2-regulated CDK inhibitors. KD of CDKN2B but not CDKN1A reversed the effect of Klf2 depletion in ECs under high flow (Fig. 7 *H* and *I*). Thus, CDKN2B down-regulation by the MEKK3-Klf2 pathway, with subsequent CDK2 activation, mediates Smad2/3 linker phosphorylation and inhibition at high FSS.

CDK Inhibition In Vivo. Lastly, we asked whether this pathway operates in vivo. Flavopiridol has been used in human clinical trials for cancer patients (32, 35). However, this compound has a short half-life in the circulation (~30 min). We, therefore, injected mice intraperitoneally (IP) with a high dose (7.5 mg/kg) of flavopiridol and examined tissues at 4 h. Endothelium from the arteries in the lungs and the femoral artery showed several fold increases in p-Smad2 nuclear staining (Fig. 8 *A–D*). These results confirm the role of CDKs in preventing Smad2/3 nuclear translocation under arterial flow. Next, we addressed whether this treatment induces vessel remodeling. An initial experiment in which mice received daily IP injection of flavopiridol showed poor survival (9 out of 16 mice died by day 7). We found, however, that mice injected 2 out of 3 d showed better survival (1 out of 16 mice died). Mice therefore received injections according to this regimen for 3 wk. Based on the accompanying paper (21), in which the lung vasculature was the most susceptible to remodeling after MEKK3 ECKO, we focused on this tissue. Examination of sections through the whole lung showed significantly increased smooth muscle actin (SMA) coverage of blood vessels (Fig. 8*E*), a result that is weaker but qualitatively similar to the effects of MEKK3 ECKO. Measurement of

blood pressure in the right ventricle revealed significant elevation, again weaker but qualitatively similar to MEKK3 ECKO (Fig. 8*F*).

Together, these data define a pathway in which MEKK3-Klf2-CDK2 suppresses Smad2/3 nuclear translocation at high FSS via Smad2/3 linker phosphorylation to limit inward remodeling at physiological flow magnitudes (diagram in *SI Appendix*, Fig. S11).

Discussion

In this study, we report that low FSS activates Smad2/3 and induces nuclear translocation and gene expression to promote inward artery remodeling. FSS at 1 dynes/cm² and above triggers p-Smad2/3 C. However, high shear (≥12 dynes/cm²) suppresses the nuclear translocation of phospho-Smad2/3 and expression of target genes. This suppression occurs without reducing C-terminal phosphorylation; FSS thus activates two independent pathways, one at low shear that induces C-terminal phosphorylation and a second one at high shear that suppresses nuclear translocation. The decreased nuclear localization/increased cytoplasmic retention at high shear thus shapes the curve so that Smad2/3 signaling peaks at low levels of FSS, consistent with a signal that governs inward remodeling.

The inhibition at higher shear occurs through MEKK3. While MEKK3 was reported to control p-Smad2/3 linker residues through Erk1/2 (36) in this setting, the induction of Klf2 under flow conditions (25) appears to be its major mode of action. Klf2, in turn, down-regulates CDKN2B, leading to the activation of CDK2. This kinase is an established Smad linker region kinase; thus, its activation inhibits nuclear translocation and signaling (26, 27). Consistent with this model, the inhibition of CDK2 results in the activation of Smad2/3 in vitro and in vivo. However, at early times after the onset of flow, the depletion of MEKK3
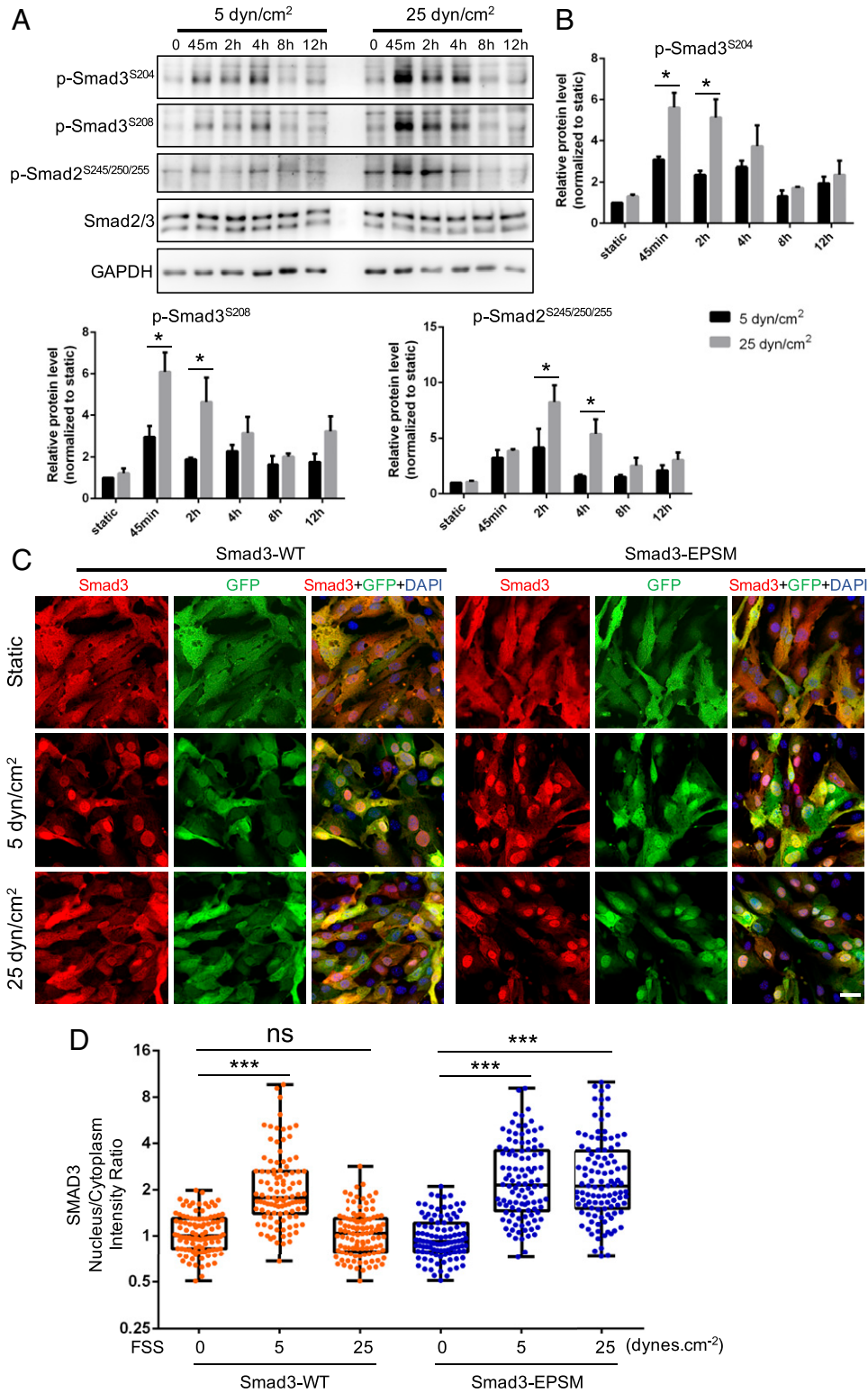
Fig. 5. Smad2/3 linker phosphorylation. (*A*) Representative Western blot of Smad2/3 linker phosphorylation (p-Smad2$^{S245/250/255}$, p-Smad3^{S204}, and p-Smad3^{S208}) in HUVECs treated with low (5 dynes/cm^2) or high (25 dynes/cm^2) FSS at different time points (static, 45 min, 2 h, 4 h, 8 h, and 12 h). (*B*) Densitometric quantification of p-Smad2$^{S245/250/255}$, p-Smad3^{S204}, and p-Smad3^{S208}; $n = 3$ independent experiments. Data represent mean ± SEM. (*C*) Representative images of Smad3 staining under static, 5 dynes/cm^2, and 25 dynes/cm^2 shear stress. Mouse aortic ECs were infected with GFP-tagged, wide-type Smad3 and linker phosphorylation sites mutant Smad3 (Smad3-EPSM). Three days later, cells were exposed to laminar FSS for 12 h, fixed, and stained for Samd2/3. (Scale bar, 25 μm.) (*D*) Quantification of Smad3 nucleus/cytoplasm intensity ratio. $n = 100$ to 150 cells for each group from three independent experiments. *$P < 0.05$, **$P < 0.01$, ***$P < 0.001$, and ns: not significant, calculated by two-way ANOVA with Sidak's multiple comparison tests (*B*) and one-way ANOVA with Tukey's multiple comparison tests (*D*).

Deng et al.
Activation of Smad2/3 signaling by low fluid shear stress mediates artery inward remodeling

PNAS | 7 of 12
https://doi.org/10.1073/pnas.2105339118

reduces Smad2/3 linker phosphorylation, whereas the depletion of Klf2 did not. This result is consistent with the slower activation of Cdk2 by flow. The data, therefore, support a model in which MEKK3 inhibits Smad2/3 via both MAP kinase activation and via the induction of Klf2 and activation of Cdk2, with the latter being more important.
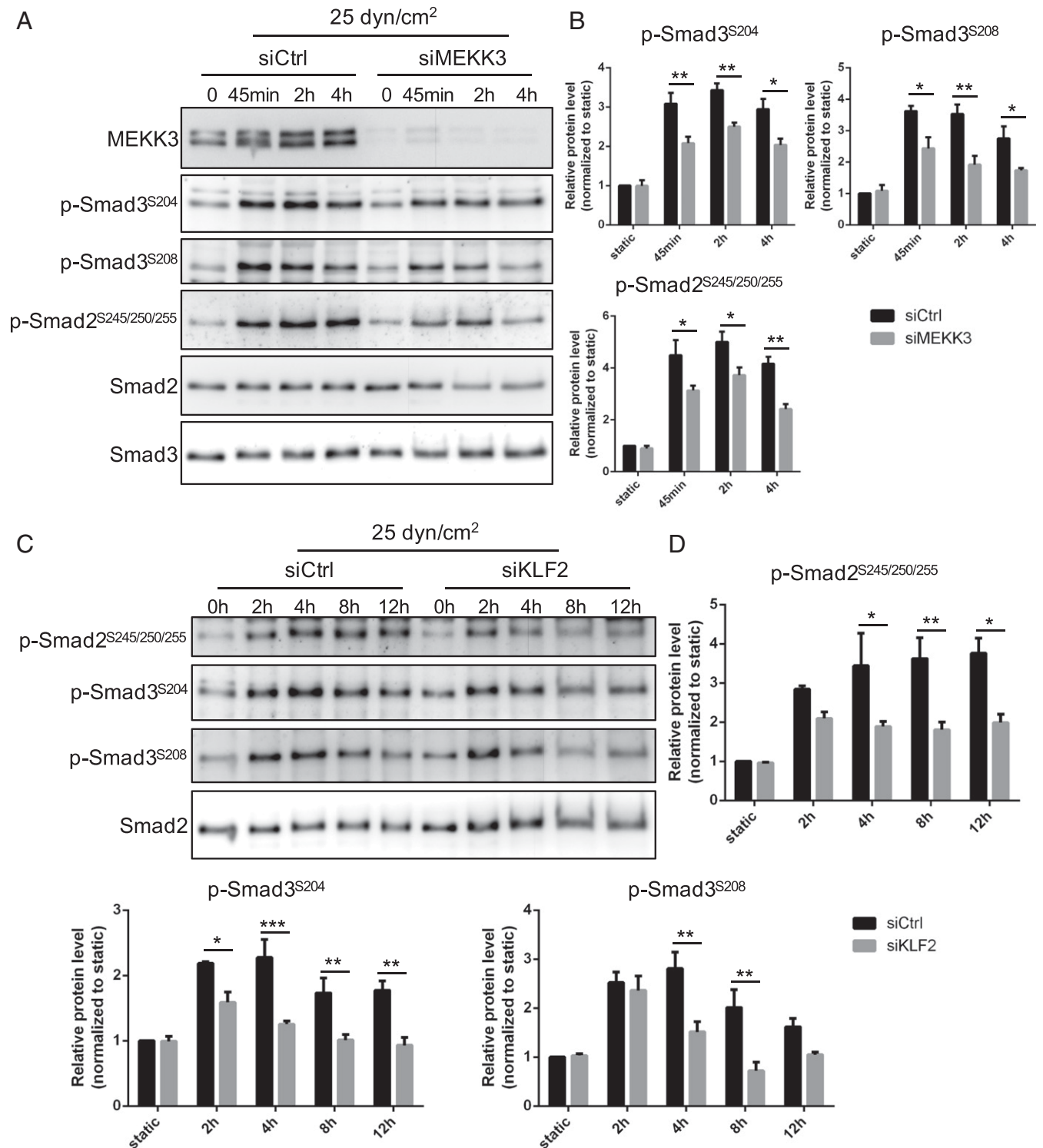

Fig. 6. MEKK3 and Klf2 regulate linker phosphorylation. (*A*) Representative Western blot of Smad2/3 linker phosphorylation (p-Smad2$^{S245/250/255}$, p-Smad3^{S204}, and p-Smad3^{S208}) in HUVECs treated with control or MEKK3 siRNA under high (25 dynes/cm^2) FSS at different time points (static, 45 min, 2 h, and 4 h). (*B*) Densitometric quantification of p-Smad2$^{S245/250/255}$, p-Smad3^{S204}, and p-Smad3^{S208}; $n = 3$ independent experiments. Data represent mean ± SEM. (*C*) Representative Western blot of Smad2/3 linker phosphorylation (p-Smad2$^{S245/250/255}$, p-Smad3^{S204}, and p-Smad3^{S208}) in HUVECs treated with control or KLF2 siRNA under high (25 dynes/cm^2) FSS at indicated time points. (*D*) Densitometric quantification of p-Smad2$^{S245/250/255}$, p-Smad3^{S204}, and p-Smad3^{S208}; $n = 3$ independent experiments. Data represent mean ± SEM. *$P < 0.05$, **$P < 0.01$, and ***$P < 0.001$, calculated by two-way ANOVA with Sidak's multiple comparison tests.
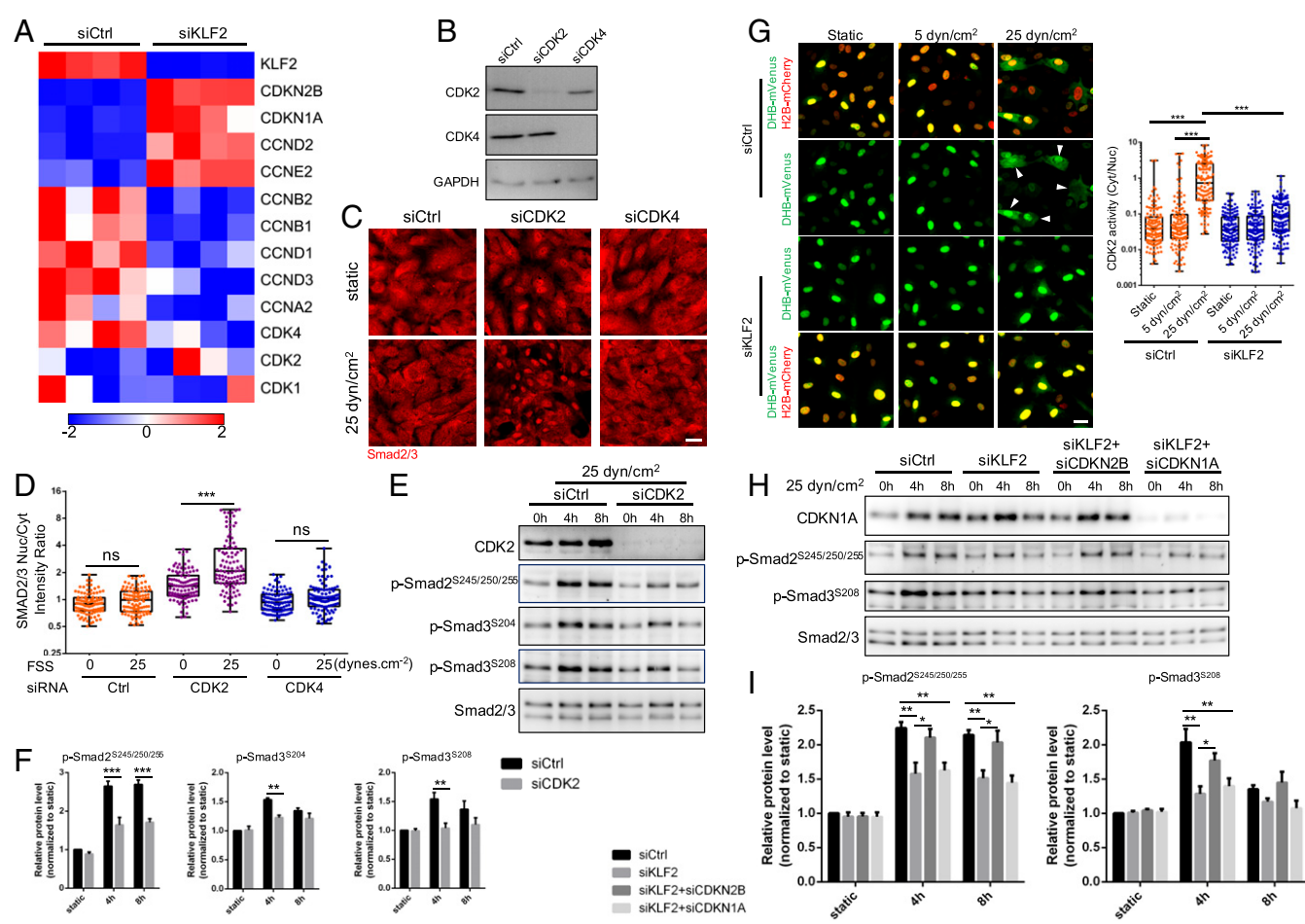
Fig. 7. CDK2 mediates Smad2/3 inhibition at high FSS. (*A*) Heat map for the expression of cell cycle regulators after Klf2 KD; $n = 4$ samples in each group. Color key shows log2 change after Klf2 depletion. (*B*) Western blot confirming CDK2 and CDK4 KD efficiency. (*C*) Representative Smad2/3 staining under static and 25 dynes/cm^2 FSS in HUVECs treated with Ctrl, CDK2, or CDK4 siRNA. (Scale bar, 50 μm.) (*D*) Quantification of Smad2/3 nucleus/cytoplasm intensity ratio. $n = 100$ to 150 cells for each group from three independent experiments. (*E*) Representative Western blot of indicated Smad2/3 linker phosphorylation in HUVECs treated with Ctrl and CDK2 siRNA under high (25 dynes/cm^2) FSS at indicated time points. (*F*) Densitometric quantification of indicated Smad2/3 linker phosphorylation; $n = 3$ independent experiments. Data represent mean ± SEM. (*G*) To assay Cdk2 activity, cells were cotransfected with the DHB-venus biosensor and histone 2B (H2B)-mCherry to mark the nuclei. Active Cdk2 phosphorylates the DHB moiety, leading to its nuclear export. Cells were subjected to FSS for 6 h at 5 or 25 dynes/cm^2, as indicated, then fixed and images taken. Ratio of cytoplasmic/nuclear signal was quantified and graphed. (*Left*) Representative images of DHB-mVenous and H2B-mCherry in HUVECs treated with control or KLF2 siRNA. (Scale bar, 50 μm.) Arrowheads are CDK2 high-activity cells. (*Right*) Quantification of CDK2 activity (cytoplasm/nucleus intensity ratio). $n = 120$ cells for each group from three independent experiments. (*H*) Representative Western blot of indicated Smad2/3 linker phosphorylation in HUVECs treated with Ctrl, KLF2, KLF2 plus CDKN2B, and KLF2 plus CDKN1A siRNA under high (25 dynes/cm^2) FSS at indicated time points. (*I*) Densitometric quantification of indicated Smad2/3 linker phosphorylation; $n = 3$ independent experiments. Data represent mean ± SEM. *$P < 0.05$, **$P < 0.01$, ***$P < 0.001$, and ns: not significant, calculated by one-way ANOVA with Tukey's multiple comparison tests (*D* and *G*) and two-way ANOVA with Sidak's multiple comparison tests (*F* and *I*).

The accompanying paper (21) reports that the EC-specific deletion of MEKK3 in mice activates Smad2/3 and induces drastic inward arterial remodeling, with resultant hypertension. This effect occurs first and most strongly in the pulmonary vasculature. These in vivo conditions correspond to the in vitro high-shear condition, in which MEKK3 was depleted (Fig. 4). Inward remodeling was blocked by Alk5 ECKO (21), providing further support for the in vivo relevance of the pathway defined here. Alk5 ECKO also blocked the inward remodeling induced by low flow in the partial carotid ligation model (Fig. 3). Together, these results elucidate an FSS signaling network that defines the shear stress set point, stabilizing the vasculature at physiological shear and inducing inward remodeling at low shear (*SI Appendix*, Fig. S11).

These findings suggest a connection between artery remodeling and the cell cycle. Recent work has shown that arterial specification, which is associated with high FSS, requires cell

cycle arrest, specifically in late G1 (31). Physiological FSS is well known to induce cell cycle arrest, though the specific phase has not been explored (reviewed in ref. 37). The activation of CDK2 appears paradoxical in light of cell cycle arrest; however, the nature of late G1 arrest is poorly understood. These considerations suggest the likely interdependence between Smad signaling, cell cycle, arterial gene expression, and vessel remodeling. The elucidation of this network is an important area for further studies.

The notion that EC flow sensing governs the remodeling of large arteries raises the question, how do ECs control the cells of the media and adventitia to affect this process? While answering this question is clearly a major task for future work, as an initial effort we examined the ECs genes regulated by TGF-β (38) and by Klf2 (*SI Appendix*, Table S1) for potential regulators of SMC behavior. Cell surface or secreted proteins regulated in the appropriate way under both conditions include Jag1 and Jag2 that
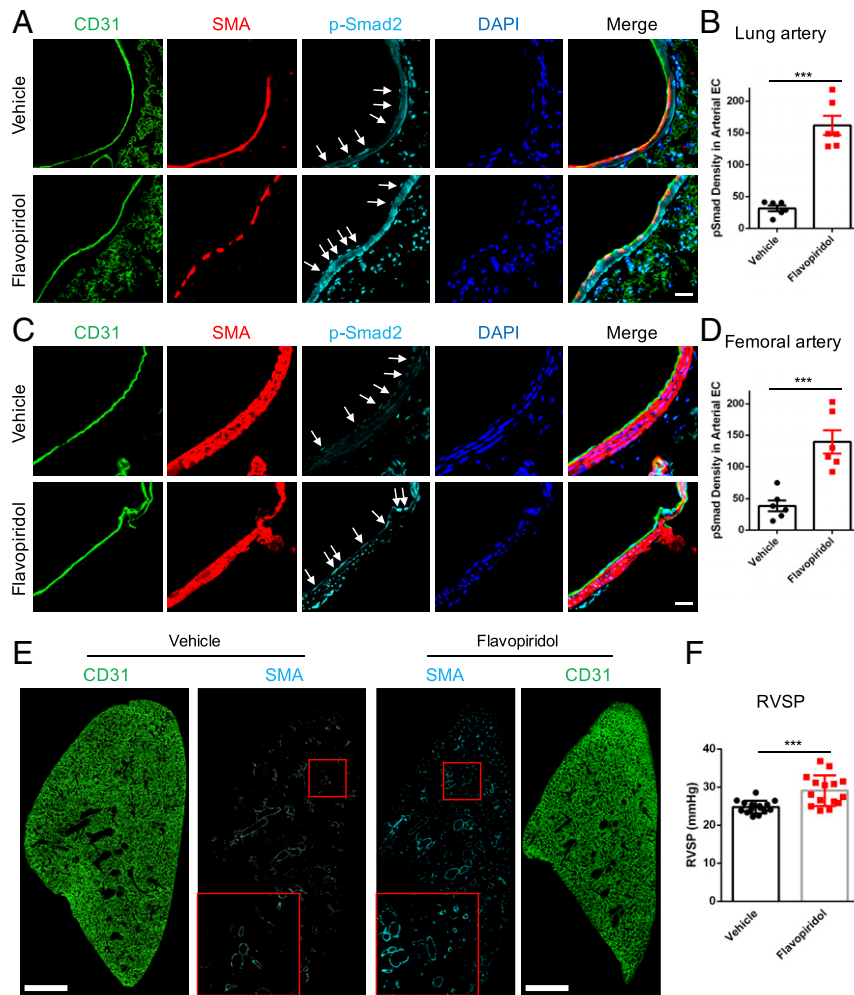
Deng et al.
Activation of Smad2/3 signaling by low fluid shear stress mediates artery inward remodeling

PNAS | 9 of 12
https://doi.org/10.1073/pnas.2105339118

CELL BIOLOGY

Fig. 8. CDK inhibition in vivo. (*A*) Representative images of p-Smad2, CD31, and SMA staining in lung arteries from vehicle- or flavopiridol-treated mice. Mice were injected IP with vehicle or flavopiridol (7.5 mg/kg) and euthanized at 4 h. Tissues were excised and fixed, and sections from lungs were stained, as indicated. Arrowheads are p-Smad2 staining in artery ECs. (Scale bar, 25 μm.) (*B*) Quantification of p-Smad2 density in lung arterial EC; *n* = 6 mice for each group. Data represent mean ± SEM. (*C*) Representative images of p-Smad2, CD31, and SMA staining in the femoral artery from vehicle- or flavopiridol-treated mice. Arrowheads are p-Smad2 staining in artery ECs. (Scale Bar, 25 μm.) (*D*) Quantification of p-Smad2 density in femoral arterial EC; *n* = 6 mice for each group. Data represent mean ± SEM. (*E*) Representative images of SMA and CD31 immunostaining in lung treated with vehicle or flavopiridol. Mice were injected with vehicle or flavopiridol, as in *A*, on a schedule with 2 d on and 1 d off for 3 wk. (Scale bar, 1 mm.) (*F*) Right ventricular systolic pressure (RVSP) of vehicle- or flavopiridol-treated mice for 3 wk. *n* = 15 mice for each group. Data represent mean ± SD. ***$P < 0.001$, calculated by unpaired *t* tests.

signal via Notch receptors; endothelin1 and NOS3 that control SMC contractility; SLIT2 and SLIT3 that signal via Robo receptors; multiple PDGF isoforms that control SMC growth and migration; MMPs and TIMPs that are critical in matrix remodeling; and multiple inflammatory factors that may act directly on SMCs or indirectly via the recruitment of monocytes and other immune cells that can then secrete additional factors. Most likely, many or all of these pathways work together to regulate the highly complex process of tissue remodeling.

Smad2/3 activation by flow is due to a shift in the dose response for BMP9, a known ligand for Alk5. BMP9 is synthesized mainly in the liver and circulates at high levels in early embryos, with lower but significant levels through adulthood (39). Although BMP10 has 65% sequence similarity and is functionally similar in terms of Smad1/5/8 activation, our results show no detectable contribution to flow-dependent Smad2/3 activation. Our data also identify Alk5 and Nrp1 as the key receptors in the flow-dependent activation of Smad2/3. This effect is quite specific, as neither receptor has a role in the activation of Smad1/5 by flow or by BMP9. While Alk5 is well known to activate

Smad2/3 (8), including in response to BMP9 (40), the involvement of Nrp1 was unexpected. However, Nrp1 both interacts with Alk5 and Alk1 in response to ligands (16) and is essential for shear stress responses involving VEGF receptors (18). Furthermore, VEGF receptor expression levels determine the FSS set point in different types of ECs (6). Future work will be required to elucidate the molecular mechanisms by which Nrp1 mediates the flow activation of this pathway.

These results shed light on the role of pathological Smad2/3 activation in arteries. While the activation of Smad2/3 in regions of low/disturbed flow likely contributes to the initiation of atherosclerotic lesions (14), in more advanced plaques, inflammatory cytokines are likely the main drivers. Factors such as IL1-β, TNF-α, and interferons sensitize ECs to TGF-β, thus allowing the activation of Smad2/3 signaling (38, 41). Strong and persistent activation of Smad2/3 signaling promotes endothelial–mesenchymal transition, more severe inflammation, and pathological vessel wall remodeling. Thus, in this setting, Smad2/3 appears to be part of a circuit that promotes disease progression. Importantly, Smad2/3 activation in diseased arteries strongly

correlates with decreased lumen diameter, ultimately closing or restricting arteries even without apparent rupture or thrombosis (3). The finding that Smad2/3 promotes inward artery remodeling may thus explain clinical progression in severe artery disease. According to this model, physiological artery remodeling in low FSS activates Smad2/3 signaling, which induces inward remodeling to restore FSS to physiological levels, which inhibits Smad2/3 and restores normal vessel stability and function. Smad2/3 activation is thus transient. In diseased arteries, inflammatory mediators induce the sustained activation of Smad2/3. Inflammatory pathways also limit Klf2 expression (42), which may further increase Smad2/3 signaling, leading to inward remodeling and the restriction of blood flow. Elucidating these molecular mechanisms in greater detail and their clinical consequences is thus an important direction for future research.

Materials and Methods

Cell Culture. Primary HUVECs were obtained from the Yale Vascular Biology and Therapeutics core facility. Each batch consists of cells isolated and pooled from three different deidentified donors. Cells were cultured in M199 (Gibco) supplemented with 20% fetal bovine serum (FBS), 1× penicillin–streptomycin (Gibco; 15140122), 100 μg/mL heparin (Sigma), and 150 μg/mL endothelial cell growth supplement (ECGS); (referred to as complete M199). HUVECs were used between passages three and six for experiments. CDK inhibitors were obtained from Selleckchem.

Shear Stress. HUVECs were seeded on tissue culture plastic slides coated with 20 μg/mL fibronectin for 2 h at 37 °C and grown to confluence. For short-term experiments, cells were starved for at least 4 h in complete M199 medium diluted 10-fold with serum-free M199 to obtain a final concentration of 2% FBS. Shear stress with a calculated intensity of 1 to 30 dyn/cm^2 was applied in parallel flow chambers, as described (11, 43), for the indicated times. For shear stress experiments conducted with ligands or blocking antibodies, HUVECs were starved for 4 h in serum-free M199 medium containing 0.2% bovine serum albumin. Recombinant human BMP9 (R&D; 3209-BP-010), BMP10 (R&D; 2926-BP-025), or TGF-β2 (R&D; 302-B2-002) were added in the indicated amounts. BMP9 and BMP10 blocking antibodies (44) were generously provided by Genentech.

siRNA Transfection. HUVECs were transfected using RNAiMax (Invitrogen; 13778100) in Opti–minimal essential medium (MEM) (Gibco; 31985070) at a final siRNA concentration between 10 to 15 nM, according to the manufacturer's instructions. EC growth medium 2 was replaced with complete M199 12 h after transfection. Cells were used for experiments 3 to 4 d after transfection. ON-TARGET Plus Smartpool siRNAs from Dharmacon were used against human Smad2 (L-003561-00-0005), human Smad3 (L-020067-00-0005), human ALK5 (L-003929-00-0005), human Nrp1 (L-019484-00-0005), human MEKK3 (L-003301-00-0005), mouse Mekk3 (L-040123-00-0005), human KLF2 (L-006928-00-0005), human CDK2 (L-003236-00-0005), human CDK4 (L-003238-00-0005), human CDKN2B (L-003245-00-0005), and human CDKN1A (L-003471-00-0005).

Lentiviral Transduction. The 293T× cells were cultured in Dulbecco's modified Eagle's medium (Gibco) supplemented with 10% FBS and 1× penicillin–streptomycin (Gibco; 15140122). At least 24 h before transfection, they were transferred to medium without antibiotics. For virus production, cells were transfected with lentiviral plasmids and packaging plasmids using Lipofectamine 2000 (Thermo Fisher Scientific; 11668010), according to the manufacturer's instructions in Opti-MEM medium (Gibco; 31985070). Supernatants containing lentivirus was collected 36 to 72 h after transfection, passed through a 0.22-μm filter, and added to HUVECs. Polybrene was added at a final concentration of 8 μg/mL to maximize transduction efficiency. HUVECs were incubated with the virus for 24 h and plated for siRNA transfection 3 to 5 d after transduction.

Reverse Transcription and qPCR. To assay gene expression, HUVECs were washed with phosphate-buffered saline (PBS) and messenger RNA (mRNA) was extracted using the RNeasy kit (Qiagen; 74106) according to the manufacturer's instructions. The complementary DNA was synthesized (Bio-Rad; 170–8890) and used for qPCR analysis (Bio-Rad; 172–5121) using Bio-Rad CFX94, according to manufacturer's instructions. Primers used for qPCR include human GAPDH (forward 5′ GTCGCTGTTGAAGTCAGAGG 3′ and reverse 5′ GAAACTGTGGCGTGATGG 3′), human fibronectin (forward 5′ AAACTTGCATCTGGAGGCAAACCC 3′ and reverse 5′ AGCTCTGATCAGCATGGACCACTT 3′),

and human integrin α5 (forward 5′ ATAGGGTGACTTGTGTTTTTAGG 3′ and reverse 5′ AAAGACATGATTGCTAAGGTCC 3′). The mRNA expression for each gene was normalized to the expression of endogenous GAPDH, and relative expression level was calculated using the ΔΔCt method. PCR amplification consisted of 5 min of an initial denaturation step at 95 °C, followed by 35 cycles of PCR at 95 °C for 15 s and 60 °C for 30 s.

Immunofluorescence. HUVECs were washed with PBS, fixed for 10 min with 3.7% PFA in PBS, permeabilized for 10 min with 1% Triton X-100 in PBS, blocked for 30 min with Starting Block blocking buffer (Thermo Fisher Scientific; 37542) at room temperature, and incubated in primary Smad2/3 antibody (1:500; Cell Signaling; #8685S) diluted in the Starting Block overnight at 4 °C. Cells were washed with PBS, incubated with secondary antibody and DAPI for 2 h at room temperature, washed again with PBS, and mounted. Images were captured with a 20× objective on a PerkinElmer spinning disk confocal microscope. Image analysis of Smad translocation was performed as described (45).

Western Blotting. HUVECs were washed with PBS and extracted in Laemmli sample buffer. Samples were run on sodium dodecyl sulfate–polyacrylamide electrophoresis gels and transferred onto nitrocellulose membranes. Membranes were blocked with 5% milk in tris-buffered saline (TBS) with Tween 20 and probed with primary antibodies overnight at 4 °C. Primary antibodies used were the following: Smad1 (1:1,000; Cell Signaling; #9743), Smad2/3 (1:1,000; Cell Signaling; #8685S), p-Smad1/5/8 (1:1,000; Cell Signaling; #13820), p-Smad2/3 (1:1,000; Cell Signaling; #8828), p-Smad2 Ser245/250/255 (1:1,000; Cell Signaling; #3104), Alk1 (1:1,000; R&D; #AF370), Alk5 (1:500; Abcam; #31013), Nrp1 (1:2,000; Cell Signaling; #3725), endoglin (1:2,000; R&D; #AF1097), actin (1:5,000; Santa Cruz; #130656), vinculin (1:5,000; Sigma; #V9131), MEKK3 (1:1,000; R&D Systems; #MAB6095), KLF2 (1:1,000; Abcam; #ab17008), GAPDH (1:5,000; Cell Signaling; #5174), eNOS (1:2,000; BD; #610297), CDK2 (1:5,000; Cell Signaling; #5174), CDK4 (1:5,000; Cell Signaling; #5174), and CDKN1A (1:5,000; Cell Signaling; #5174). HRP-conjugated mouse secondary (Vector Laboratories; #PI-2000) and rabbit secondary (Vector Laboratories; PI-1000) antibodies were used at 1:10,000.

RNAseq. Total RNA was extracted from HUVECs treated with control or KLF2 siRNA and quantitated by NanoDrop. RNA integrity number value was measured with an Agilent Bioanalyzer. Samples were subjected to RNAseq using Illumina NextSEq. 500 sequencer (75 bp paired end reads). The base calling data from the sequencer were transferred into FASTQ files using bcl2fastq2 conversion software (version 2.20, Illumina). The raw reads were aligned to the human reference genome GRCh38 using HISAT2 (version 2.1.0) alignment software. The raw reads were processed using HTSeq (version 0.11.1) to generate read counts for every gene. DESeq2 (version 1.24, using default parameter) was used to preprocess raw data to remove the noise, normalize each sample to correct the batch effect, perform principal component analysis for observing the similarity of replicates, and identify differential expression genes. P values obtained from multiple tests were adjusted using Benjamini–Hochberg correction.

Animals. Eight-week-old male and female C57BL/6J mice (Charles River Laboratories) were used in this study. These mice were housed in groups in a light (12-h light cycle) and temperature (21 °C) controlled environment. They were fed a pellet rodent diet, ad libitum, and had free access to water preprocedure. The study conformed to the guidelines for the Care and Use of Laboratory Animals published by the US NIH (NIH Publication No. 85–23, revised 1985) (46) and was approved by the Institutional Animal Care and Use Committee.

Partial Ligation of the Right Carotid Artery. Mice were anesthetized using inhalation of 2% isoflurane through a vaporizer with 100% oxygen. Nair was applied in the neck between the mandible and the sternum to remove the hair. Betadine and 70% ethanol were used to sterilize the surgical area. All surgical manipulations were performed under a dissecting microscope, maintaining aseptic conditions on a heated surgical pad at 37 °C. The cervical skin was cut in the midline. Then, the right common carotid artery and its bifurcation were bluntly dissected to expose all four distal branches: external carotid artery, internal carotid artery, OA, and STA. The external carotid below the superior thyroid was tied off using 6-0 silk suture. The internal carotid distal to the OA was also tied off using 6-0 silk suture. Thus, only the OA remained patent. The skin was closed with a 6-0 prolene suture. Fully conscious animals were returned to their original cages. Buprenorphine was administered subcutaneously at 0.05 mg/kg once, preemptively, then every 12 h for 72 h. The survival rate for the surgery was 94%.

Carotid Ultrasound Examination. To validate whether the partial ligation reduced flow, carotid flow was examined utilizing a commercially available system (the Vevo 770, Fujifilm, Visualsonics Inc.) 1 d postligation. Mice were positioned on an imaging stage with a heating system to maintain physiological body temperatures during imaging. Electrocardiographic leads were attached to each limb. Pulse wave Doppler was also recorded in a paratrachea long-axis views in both the right and left common carotid. Images from these studies were recorded digitally for subsequent analysis. Successful partial carotid ligation was indicated by overall reduction in flow (~80 to 90%) in the right common carotid, compared with the left side, with reversal of flow toward aortic inlet during diastole.

Blood Pressure Measurement. Right ventricular systolic pressure was measured with a 1.4-F pressure transducer catheter (Millar Instruments) and recorded by LabChart software (ADInstruments). Briefly, mice were anesthetized with 2% isoflurane, then the catheter was inserted through the right jugular vein into the right ventricle.

Immunohistology. Carotid arteries were harvested after euthanasia. Briefly, animals were first perfused with PBS then with a fixative solution (4% PFA) by injection through the cardiac left ventricle. Arteries were then removed, further fixed in 4% PFA for 2 h, and embedded in paraffin. Thin transverse sections (5 μm) were cut approximatively 5 mm upstream of the ligation site. Sections were then deparafinized and rehydrated. Antigens were recovered by immersion for 20 min in an ethylenediaminetetraacetic acid buffer at pH 8 at 98 °C. Slides were then blocked with SuperBlock TBS buffer (Thermo Fisher Scientific) for 1 h. Slides were incubated overnight at 4 °C with primary p-Smad2 (Thermo Fisher Scientific; #4–244G), SMA (Sigma; #A5228), PECAM-1 (R&D; #AF3628), and Nrp1 (R&D; AF556) antibodies diluted 1:200 in blocking buffer. Samples were washed 4× then incubated with secondary antibodies (1:400, donkey anti-mouse AlexaFluor 568, donkey anti-rabbit AlexaFluor 647, and molecular probes; Thermo Fisher Scientific). Slides were then mounted in Fluoromount-G (Southern Biotech).

1. C. Michiels, Physiological and pathological responses to hypoxia. *Am. J. Pathol.* **164**, 1875–1882 (2004).
2. G. H. Gibbons, V. J. Dzau, The emerging concept of vascular remodeling. *N. Engl. J. Med.* **330**, 1431–1438 (1994).
3. N. Baeyens, C. Bandyopadhyay, B. G. Coon, S. Yun, M. A. Schwartz, Endothelial fluid shear stress sensing in vascular health and disease. *J. Clin. Invest.* **126**, 821–828 (2016).
4. A. Kamiya, T. Togawa, Adaptive regulation of wall shear stress to flow change in the canine carotid artery. *Am. J. Physiol.* **239**, H14–H21 (1980).
5. B. L. Langille, F. O'Donnell, Reductions in arterial diameter produced by chronic decreases in blood flow are endothelium-dependent. *Science* **231**, 405–407 (1986).
6. N. Baeyens *et al.*, Vascular remodeling is governed by a VEGFR3-dependent fluid shear stress set point. *eLife* **4**, e04645 (2015).
7. J. Nickel, P. Ten Dijke, T. D. Mueller, TGF-β family co-receptor function and signaling. *Acta Biochim. Biophys. Sin. (Shanghai)* **50**, 12–36 (2018).
8. F. Lebrin, M. Deckers, P. Bertolino, P. Ten Dijke, TGF-beta receptor function in the endothelium. *Cardiovasc. Res.* **65**, 599–608 (2005).
9. P. ten Dijke, C. S. Hill, New insights into TGF-beta-Smad signalling. *Trends Biochem. Sci.* **29**, 265–273 (2004).
10. A. Hata, Y.-G. Chen, TGF-β signaling from receptors to Smads. *Cold Spring Harb. Perspect. Biol.* **8**, a022061 (2016).
11. N. Baeyens *et al.*, Defective fluid shear stress mechanotransduction mediates hereditary hemorrhagic telangiectasia. *J. Cell Biol.* **214**, 807–816 (2016).
12. N. W. Morrell *et al.*, Targeting BMP signalling in cardiovascular disease and anaemia. *Nat. Rev. Cardiol.* **13**, 106–120 (2016).
13. T.-L. Yang *et al.*, Differential regulations of fibronectin and laminin in Smad2 activation in vascular endothelial cells in response to disturbed flow. *J. Biomed. Sci.* **25**, 1 (2018).
14. P.-Y. Chen *et al.*, Endothelial-to-mesenchymal transition drives atherosclerosis progression. *J. Clin. Invest.* **125**, 4514–4528 (2015).
15. P.-Y. Chen *et al.*, Smooth muscle cell reprogramming in aortic aneurysms. *Cell Stem Cell* **26**, 542–557.e11 (2020).
16. I. M. Aspalter *et al.*, Alk1 and Alk5 inhibition by Nrp1 controls vascular sprouting downstream of Notch. *Nat. Commun.* **6**, 7264 (2015).
17. A. Lanahan *et al.*, The neuropilin 1 cytoplasmic domain is required for VEGF-A-dependent arteriogenesis. *Dev. Cell* **25**, 156–168 (2013).
18. V. Mehta *et al.*, The guidance receptor plexin D1 is a mechanosensor in endothelial cells. *Nature* **578**, 290–295 (2020).
19. Z. Chen, E. Tzima, PECAM-1 is necessary for flow-induced vascular remodeling. *Arterioscler. Thromb. Vasc. Biol.* **29**, 1067–1073 (2009).
20. D. Nam *et al.*, Partial carotid ligation is a model of acutely induced disturbed flow, leading to rapid endothelial dysfunction and atherosclerosis. *Am. J. Physiol. Heart Circ. Physiol.* **297**, H1535–H1543 (2009).
21. H. Deng *et al.*, MEKK3-TGFβ crosstalk regulates inward arterial remodeling. bioRxiv [Preprint] (2021). https://doi.org/10.1101/2021.08.19.456893 (Accessed 2 September 2021).
22. G. N. Nithianandarajah-Jones, B. Wilm, C. E. P. Goldring, J. Müller, M. J. Cross, The role of ERK5 in endothelial cell function. *Biochem. Soc. Trans.* **42**, 1584–1589 (2014).
23. R. C. Looft-Wilson, J. E. Billig, W. C. Sessa, Shear stress attenuates inward remodeling in cultured mouse thoracodorsal arteries in an eNOS-dependent, but not hemodynamic manner, and increases Cx37 expression. *J. Vasc. Res.* **56**, 284–295 (2019).
24. Y. Castier, R. P. Brandes, G. Leseche, A. Tedgui, S. Lehoux, p47phox-dependent NADPH oxidase regulates flow-induced vascular remodeling. *Circ. Res.* **97**, 533–540 (2005).
25. R. A. Boon, A. J. G. Horrevoets, Key transcriptional regulators of the vasoprotective effects of shear stress. *Hamostaseologie* **29**, 39–43 (2009).
26. D. Kamato *et al.*, Transforming growth factor-β signalling: Role and consequences of Smad linker region phosphorylation. *Cell. Signal.* **25**, 2017–2024 (2013).
27. I. Matsuura *et al.*, Cyclin-dependent kinases regulate the antiproliferative function of Smads. *Nature* **430**, 226–231 (2004).
28. F. Huang *et al.*, HER2/EGFR-AKT signaling switches TGFβ from inhibiting cell proliferation to promoting cell migration in breast cancer. *Cancer Res.* **78**, 6073–6085 (2018).
29. P. G. Wyatt *et al.*, Identification of N-(4-piperidinyl)-4-(2,6-dichlorobenzoylamino)-1H-pyrazole-3-carboxamide (AT7519), a novel cyclin dependent kinase inhibitor using fragment-based X-ray crystallography and structure based drug design. *J. Med. Chem.* **51**, 4986–4999 (2008).
30. M. D. Losiewicz, B. A. Carlson, G. Kaur, E. A. Sausville, P. J. Worland, Potent inhibition of CDC2 kinase activity by the flavonoid L86-8275. *Biochem. Biophys. Res. Commun.* **201**, 589–595 (1994).
31. N. Chavkin *et al.*, Endothelial cell cycle state determines propensity for arterial-venous fate. *bioRxiv* [Preprint] (2020). https://www.biorxiv.org/content/10.1101/2020.08.12.246512v1 (Accessed 2 September 2021).
32. G. I. Shapiro, Preclinical and clinical development of the cyclin-dependent kinase inhibitor flavopiridol. *Clin. Cancer Res.* **10**, 4270s–4275s (2004).
33. B. Barlaam *et al.*, Discovery of AZD4573, a potent and selective inhibitor of CDK9 that enables short duration of target engagement for the treatment of hematological malignancies. *J. Med. Chem.* **63**, 15564–15590 (2020).
34. S. L. Spencer *et al.*, The proliferation-quiescence decision is controlled by a bifurcation in CDK2 activity at mitotic exit. *Cell* **155**, 369–383 (2013).
35. J. F. Zeidner, J. E. Karp, Clinical activity of alvocidib (flavopiridol) in acute myeloid leukemia. *Leuk. Res.* **39**, 1312–1318 (2015).
36. X. Chang *et al.*, The kinases MEKK2 and MEKK3 regulate transforming growth factor-β-mediated helper T cell differentiation. *Immunity* **34**, 201–212 (2011).
37. H. Nakajima, N. Mochizuki, Flow pattern-dependent endothelial cell responses through transcriptional regulation. *Cell Cycle* **16**, 1893–1901 (2017).
38. P.-Y. Chen *et al.*, Endothelial TGF-β signalling drives vascular inflammation and atherosclerosis. *Nat. Metab.* **1**, 912–926 (2019).
39. L. David *et al.*, Bone morphogenetic protein-9 is a circulating vascular quiescence factor. *Circ. Res.* **102**, 914–922 (2008).
40. J. M. Muñoz-Félix *et al.*, Identification of bone morphogenetic protein 9 (BMP9) as a novel profibrotic factor in vitro. *Cell. Signal.* **28**, 1252–1261 (2016).
41. P.-Y. Chen *et al.*, FGF regulates TGF-β signaling and endothelial-to-mesenchymal transition via control of let-7 miRNA expression. *Cell Rep.* **2**, 1684–1696 (2012).
42. A. Kumar, Z. Lin, S. SenBanerjee, M. K. Jain, Tumor necrosis factor alpha-mediated reduction of KLF2 is due to inhibition of MEF2 by NF-kappaB and histone deacetylases. *Mol. Cell. Biol.* **25**, 5893–5903 (2005).
43. J. A. Frangos, S. G. Eskin, L. V. McIntire, C. L. Ives, Flow effects on prostacyclin production by cultured human endothelial cells. *Science* **227**, 1477–1479 (1985).
44. R. Ola *et al.*, PI3 kinase inhibition improves vascular malformations in mouse models of hereditary haemorrhagic telangiectasia. *Nat. Commun.* **7**, 13650 (2016).
45. N. Baeyens *et al.*, Syndecan 4 is required for endothelial alignment in flow and atheroprotective signaling. *Proc. Natl. Acad. Sci. U.S.A.* **111**, 17308–17313 (2014).
46. National Research Council, *Guide for the Care and Use of Laboratory Animals* (National Academies Press, Washington, DC, ed. 8, 2011).